Reconfigurable Chains of Bifurcating Type III Bricard Linkages

Shengnan Lu[1,2], Dimiter Zlatanov[2], Xilun Ding[1], Matteo Zoppi[2], Simon D. Guest[3]

[1]*Robotics Institute, Beihang University, China 100191, e-mail: lvshengnan5@gmail.com, xlding@buaa.edu.cn*
[2]*PMAR Robotics, University of Genoa, Italy 16145, e-mail: zlatanov, zoppi@dimec.unige.it*
[3]*Department of Engineering, University of Cambridge, UK, e-mail: sdg@eng.cam.ac.uk*

Abstract This paper presents the construction of a family of reconfigurable mechanisms composed of an unlimited number of doubly collapsible (type III) Bricard linkages. First, the geometries of these overconstrained six-hinge spatial loops are parameterized and their kinematics is investigated. The configuration-space curve is computed; its bifurcation behavior is analyzed and illustrated by projections. It is then shown that type III Bricard linkages can be connected in series in a one-degree-of-freedom chain. Such a multi-loop mechanism has the ability to reconfigure in multiple ways due to the bifurcations of the individual Bricard units. Consequently, the chain has multiple states where all joint axes are coplanar. In each such configuration, the physical links, every one realized as a planar figure, spread out to cover a curving stripe in the plane. Several simulations and case studies are performed.

Keywords Bricard linkage, bifurcation, configuration space, reconfigurable mechanism.

1 Introduction

Mechanisms whose degree-of-freedom (dof) is underestimated by the standard Grübler-Kutzbach formula are called overconstrained [1]. Starting with Sarrus [2], many spatial linkages with this fascinating property have been proposed, such as those named after Bennett, Myard, and Bricard [3].

The French engineer and geometer Raoul Bricard discovered a family of mobile 6R loops of three types: line-symmetric, plane-symmetric, and doubly collapsible [4]. Baker analyzed all types of Bricard linkages by appropriate sets of independent closure equations [5]. Luo et al. investigated the geometric configuration of the threefold-symmetric Bricard [6]. Chen and Chai discussed the bifurcation of a special Bricard linkage which is both line- and plane-symmetric [7].

This paper focuses on the type III Bricard loop. Its defining property is the existence of two collapsed configurations where all joint axes become coplanar and the system of constraints loses rank. The configuration space bifurcates and the potential motion path from that moment is not unique. This feature provides an opportunity of using the linkage to construct reconfigurable mechanisms. This is done

by forming serial chains of Bricard loops, adjacent units being joined by scissor elements so that the total dof remains one regardless of the length of the chain. The bifurcations of the unit linkages then cause multi-furcations of the c-space of the combined mechanism, and the potential of a large variety of paths with the same input-joint-value time history.

The paper is organized as follows. In Section 2, the type III Bricard linkage is reviewed and parameterized. Then, the configuration space and its bifurcation is analyzed in Section 3. Section 4 discusses the possibility of using the doubly collapsible Bricard in the design of reconfigurable mechanisms. Finally, a model of a reconfigurable mechanism, composed of type III units, is created and simulated.

2 The Type III Bricard Linkage

The Bricard linkage $ABCA'B'C'$ in Fig. 1, is of type III with two collapsed states. The linkage can be constructed as follows: draw two concentric circles of arbitrary radii; choose two arbitrary points A and A' outside the larger circle; construct the tangents from A and A' to the circles and determine their intersections B, B', C and C'. The lines BC, $B'C'$, $B'C$ and BC' will be tangent to a third concentric circle with radius r_t. Then the six triangles ABC', ABC, $A'BC$, $A'B'C$, $A'B'C'$, $AB'C'$, taken in that cyclic order and hinged at their common edges, constitute a deformable six-plate linkage with one dof [8].

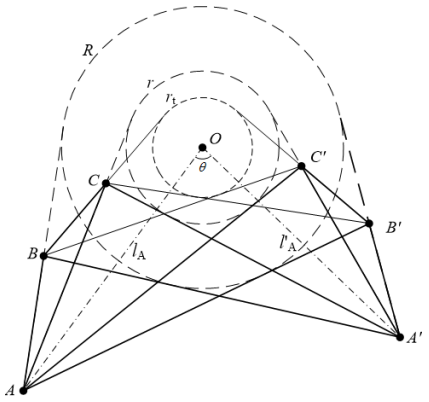

Fig. 1 Geometric construction of the type III Bricard linkage

The six triangles in fact define a deformable octahedron: the two remaining (virtual) faces are the triangles ACB' and $A'C'B$, whose shape is constant during the movement. (However, if they are physically part of the linkage, link interference is unavoidable during any finite motion.) Furthermore, any six of the eight faces can be hinged together, generating an equivalent motion of the octahedron.

From the construction in Fig. 1, a type III Bricard geometry can be decided by the radii, R and r, of the two circles and the positions of point A and A'. We denote the angle between OA and OA' with θ and their lengths as l_A and l'_A, respectively.

3 Kinematic Analysis

The configuration space of an arbitrary type III Bricard linkage is analyzed in this section, identifying clearly its bifurcation points.

3.1 Configuration Space

Generally, the configuration space of a mechanism can be described by different variables, such as angles or distances. Herein, we trace the kinematic path of point M, the midpoint of $B'C'$, to describe the configuration space of the Bricard linkage.

The triangle ABC is taken as the fixed base link. The base frame is $Axyz$ with Ay directed from A to C and Az along $\overrightarrow{AC} \times \overrightarrow{AB}$, Fig. 2.

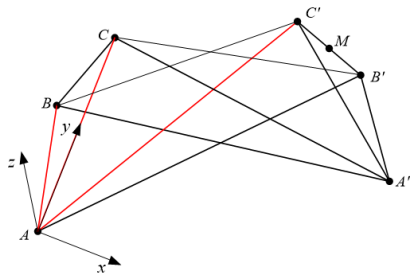

Fig. 2 Coordinate system of the Bricard linkage

As a (virtual) face of a deformable octahedron, triangle ACB' has invariant shape. Therefore, B' rotates around AC. On the other hand, the position of B' is determined by the joint-angles about the axes along AB and AC'. Therefore,

$$\mathbf{r}'_B(\sigma_3) = \exp(\sigma_3\hat{\mathbf{e}}_3)\,\mathbf{r}'_B(0) = \exp(\sigma_1\hat{\mathbf{e}}_1)\exp(\sigma_2\hat{\mathbf{e}}_2)\,\mathbf{r}'_B(0) \tag{1}$$

Above $\mathbf{r}'_B$ is the position vector of B', while σ_i is the joint angle about the axis with unit vector $\mathbf{e}_i$, $i = 1,2,3$,

$$\mathbf{e}_1 = \frac{\overrightarrow{AB}}{|AB|}, \quad \mathbf{e}_2 = \frac{\overrightarrow{AC'}}{|AC'|}, \quad \mathbf{e}_3 = \frac{\overrightarrow{AC}}{|AC|}, \tag{2}$$

and $\hat{\mathbf{e}}_i$ is the 3×3 skew-symmetric matrix obtained from $\mathbf{e}_i$. The reference configuration, where the three angle values, σ_i, are zero, is taken as in Fig. 2.

All terms in (1) are determined by the five Bricard-geometry parameters and the joint angles σ_i. In particular,

$$\mathbf{e}_1 = \begin{bmatrix} -\sin(\alpha_1-\alpha_2) \\ \cos(\alpha_1-\alpha_2) \\ 0 \end{bmatrix} \quad \mathbf{e}_2 = \begin{bmatrix} \sin 2\alpha_2 \\ \cos 2\alpha_2 \\ 0 \end{bmatrix} \quad \mathbf{e}_3 = \begin{bmatrix} 0 \\ 1 \\ 0 \end{bmatrix} \tag{3}$$

where $\alpha_1 = \angle BAC = \arcsin\dfrac{R}{l_A}$, $\alpha_2 = \angle CAB' = \arcsin\dfrac{r}{l_A}$.

As B' rotates around Ay, its y coordinate is constant. Thus, from the y-component equation in (1), we get this relation between σ_1 and σ_2:

$$k_1 + k_2 \cos\sigma_1 + k_3 \cos\sigma_2 + k_4 \cos\sigma_1 \cos\sigma_2 + k_5 \sin\sigma_1 \sin\sigma_2 = 0 \tag{4}$$

where k_1, k_2, k_3, k_4, k_5 are functions of the parameters of the Bricard linkage:

$$\begin{aligned}
k_1 &= 2Rl_A^2 r - Rr^3 - R^3 r - (R^2 l_A^2 + l_A^2 r^2) k_0 \\
k_2 &= R^3 r - Rr^3 + (R^2 l_A^2 - l_A^2 r^2) k_0 \\
k_3 &= Rr^3 - R^3 r - (R^2 l_A^2 - l_A^2 r^2) k_0 \\
k_4 &= -2Rl_A^2 r + Rr^3 + R^3 r + (R^2 l_A^2 + l_A^2 r^2) k_0 \\
k_5 &= 2R^2 r^2 - R^2 l_A^2 - l_A^2 r^2 + 2Rl_A^2 r k_0 \\
k_0 &= \sqrt{1 - \frac{R^2}{l_A^2}} \sqrt{1 - \frac{r^2}{l_A^2}}
\end{aligned}$$

It can be seen that only R, r, and l_A affect the relationship between σ_1 and σ_2. By solving (4), it is found that there are two σ_2 values in $[-\pi, \pi)$ corresponding to each σ_1, except in the two configurations where $\cos\sigma_1 = \cos\sigma_2 = \pm 1$, i.e., when $\sigma_1 = \sigma_2$ is a multiple of π. In Fig. 3, the two curves on the torus parameterized by σ_1 and σ_2 illustrate clearly the relationship between the two angles when $R = 60$, $r = 21.96$, and $l_A = 60\sqrt{2}$.

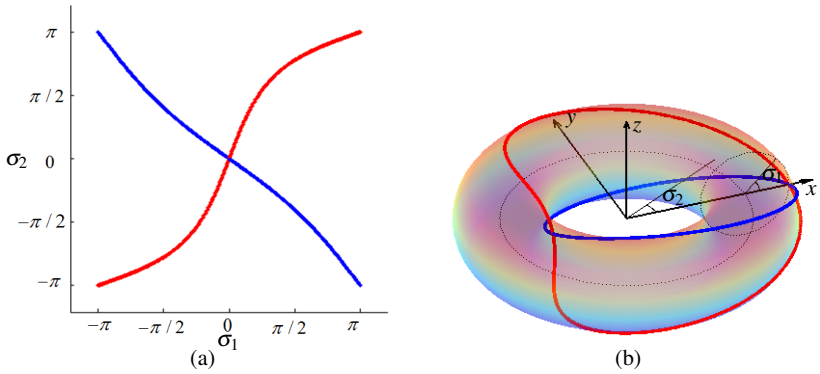

Fig. 3 Relationship between σ_1 and σ_2 on a torus

For every pair of values (σ_1, σ_2) there is no more than one feasible configuration of the linkage. Because, if σ_1 and σ_2 are given, points A, B, C, B', C' are fixed. It has been proven that the position of the remaining point A' is determined by that of the other five points in a unique way [9]. This means that the curve on the (σ_1, σ_2) torus is a one-to-one projection of the configuration space.

The configuration space of such a linkage can also be described by a system of 3 equations in the variables x_M, y_M, and z_M. The position of M, the midpoint of $A'B'$, can be calculated as

$$\mathbf{r}_M(t) = \exp(\sigma_1 \hat{\mathbf{e}}_1) \exp(\sigma_2 \hat{\mathbf{e}}_2) \mathbf{r}_M(0) \tag{5}$$

where $\mathbf{r}_M(0)$ is the position of M in the reference configuration, $\mathbf{r}_M(0) = \frac{1}{2}(\mathbf{r}'_A(0) + \mathbf{r}'_B(0))$, which is also a function of the five parameters of the Bricard linkage.

The possible trajectories of M are calculated by (5) and the result is shown in Fig. 4. Since M is on the triangular plate $AB'C'$, the trajectory of M also locates on a sphere centered at A.

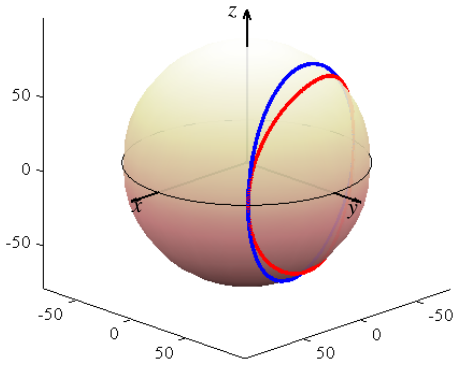

Fig. 4 Trajectory of point M

Due to the two-to-one correspondence between σ_2 and σ_1, there are two smooth possible kinematic paths of M when σ_1 cycles from 0 to 2π. Each of the curves is homeomorphic to a circle and they share exactly two points, both of which lie on the "equator" of the sphere centered at A (i.e., its intersection with Axy.). In fact, at these points the curves are tangent. Indeed, in both configurations, the linkage is collapsed and M is in the plane Axy together with all joint axes. Therefore, there is only one independent feasible velocity of M: parallel to Az.

By varying the five geometric parameters in their ranges, the topology of the configuration space of the type III Bricard linkage stays the same. It is homeomorphic to two circles fused at two points, which also agrees with the result in [10].

3.2 Bifurcation Analysis

As noted above, when $\sigma_1 = 0$ or $\sigma_1 = \pi$ only one σ_2 value is obtained. These two angles correspond to the two common points of the smooth paths of M. If motion starts at one of these two configurations, M is able to follow either curve, i.e. its path bifurcates. With only one joint input, such as σ_1, the movement of the linkage becomes uncertain.

In the following, we take the above model as an example to discuss the influence of the bifurcation on the movement of the linkage. Figure 5 displays some configurations of the Bricard linkage related to the corresponding points on its configuration-space curve.

Figures 5(a) and 5(d) show the two configurations at the bifurcation points which are in fact the two collapsed states of the Bricard linkage. At each, all the six revolute-joints axes of the linkage are coplanar, the rank of the screw system they

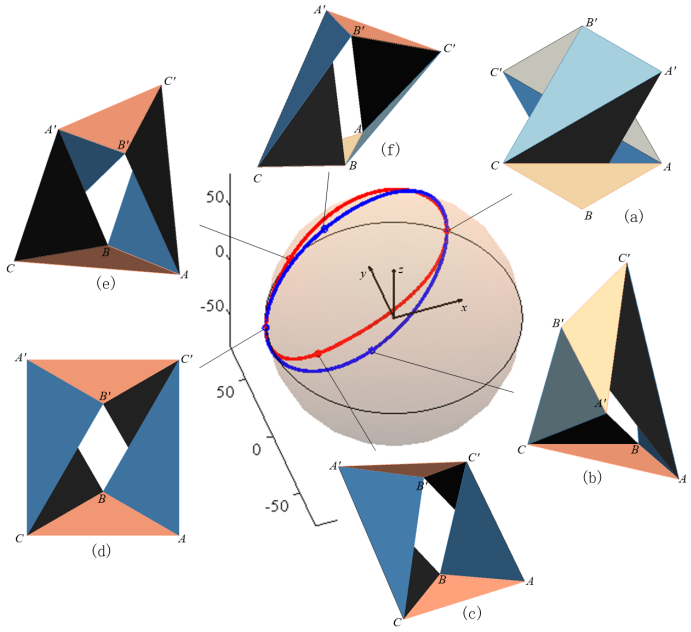

Fig. 5 Configurations of the Bricard linkage: (a) $\sigma_1 = \sigma_2 = 0$ (bifurcation point); (b) $\sigma_1 = \pi/2$, $\sigma_2 = -1.26$; (c) $\sigma_1 = \pi/2$, $\sigma_2 = 2.44$; (d) $\sigma_1 = \sigma_2 = \pi$ (bifurcation); (e) $\sigma_1 = -2\pi/3$, $\sigma_2 = -2.73$; (f) $\sigma_1 = -2\pi/3$, $\sigma_2 = 1.81$

span reduces to 3, and the instantaneous degree of freedom of the linkage increases to 3. Two of the feasible independent instantaneous motions lead to finite curves and bifurcation occurs. The configurations in Fig. 5(b) and Fig. 5(c) are distinct but correspond to the same value of σ_1. The same is true for Fig. 5(e) and Fig. 5(f).

Therefore, the type III Bricard linkage can change its kinematic path at each bifurcation point, which means the mechanism can potentially reconfigure itself.

4 Application in the Design of Reconfigurable Mechanisms

The bifurcation of the type III Bricard linkage provides a potential of using the mechanism in the design of reconfigurable deployable mechanisms. An unlimited number of linkages can be connected in a one-dof chain. Each such mechanism has a multi-furcating configuration-space curve allowing different folding shape and deploying trajectories.

4.1 Connecting Two Type III Bricard Linkages

Herein, the link panels of the linkages are supposed to be thin enough, as in a paper model; the limitation of movement generated by the thickness of the model can be ignored.

Two Bricard linkages, $ABCA'B'C'$ and $A_1B_1C_1A'_1B'_1C'_1$ can be linked together by using a common hinge, as shown in Fig. 6(a). By sharing the revolute joint AC', as well as the panels ABC' and $AB'C'$, two Bricard linkages are connected. This joining can also be seen as the adding of a scissor linkage between the two Bricard linkages. A simulated model of the assembly is shown in Fig. 6(b).

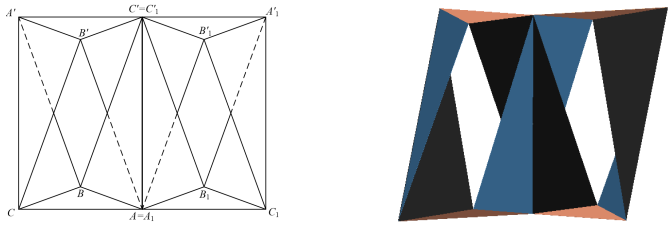

(a) (b)

Fig. 6 Two Bricard linkages connected by a scissor element

The common panels are $BC'B'_1A$ and $B_1C'B'A$ and they rotate with respect to each other around $AC' = A_1C'_1$. The joint angles of the two Bricards about this common axis are then the same (as vertical angles) and equal to σ_2 in Fig. 2. Therefore, the two linkages move synchronously and so the mobility of the combined mechanism is one. Clearly, the dof will not change if, using the same procedure, a third linkage is joined to the second, and so on. Thus, a one-dof Bricard chain of arbitrary length can be constructed.

4.2 Construction of Reconfigurable Mechanisms

As discussed in Subsection 3.2, the kinematic path of the Bricard linkage bifurcates into two branches at two points. With the exception of the two bifurcation points, there are two configurations corresponding to a given input at any revolute joint.

Even if two type III Bricard linkages trace different trajectories, whenever their σ_2 angle is the same, they can be connected together by the above method, despite the fact that their configurations may be on different branches of the configuration space. Therefore, for an assembly of two Bricard linkages, there will be 4 possible trajectories from an initial collapsed state when one joint angle is driven. For a chain of length n, the configuration space multi-furcates into 2^n branches. All the linkages arrive at collapsed configurations at the same time for any trajectory. However, these states maybe quite different for two c-space paths of the same mechanism. In other words, we have a potentially highly-reconfigurable deployable mechanism, which can be used for multiple different folding (or unfolding) sequences.

Figure 7 shows a motion sequence of such a mechanism composed of four Bricard linkages. The unit Bricard linkage has a rectangular outline. The mechanism is at a coplanar configuration in Fig. 7(a), the outline is a rectangle (with area four times the area of the unit). Starting from this configuration, different kinematic paths can be followed. Some examples are shown in Figs. 7(b), 7(c), and 7(d). The configuration in the other coplanar state is also given in the figures. Although

the initial configuration of the mechanisms is the same, as they are tracing various trajectories, the configurations at the next bifurcation point are different.

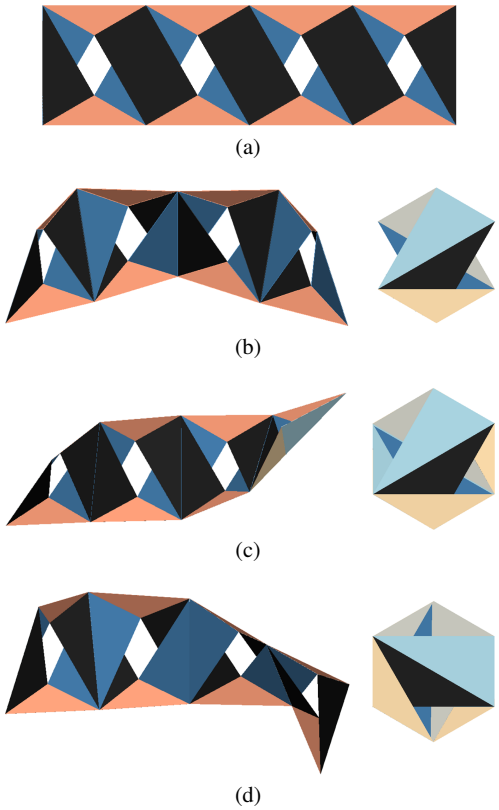

Fig. 7 Motion sequences of a reconfigurable chain consisting of four Bricard linkages

5 Case study

Two paper models of reconfigurable mechanisms, each composed of three type III Bricard linkages, are made. The unit linkage has a rectangular outline, $R = 80$, $r = 47.81$, $l_A = l'_A = 80\sqrt{2}$ and $\theta = 20^\circ$. The configurations, where all the revolute joints are coplanar, are shown in Fig. 8. In each subfigure, the state with $\sigma_1 = \sigma_2 = \pi$ is on the left and $\sigma_1 = \sigma_2 = 0$ is on the right.

The physical shapes of the links affect the motion range of the linkage and limit the possible kinematic paths. In the left-hand side of Fig. 8(a) (where $\sigma_1 = \sigma_2 = \pi$) the paper panel $AB'C'$ is on top of ABC'. Since the panels cannot cross, to avoid physical interference in any motion from this configuration σ_2 can only change in the negative direction, becoming smaller than π. In other words, the model can move from the configuration in Fig. 5(d) to the ones in Fig. 5(c) and (f), but not to Fig. 5(e) or (b). In Fig. 8(b), ABC' is on top and so σ_2 must increase and become larger than

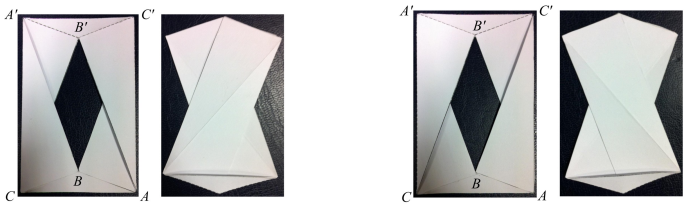

Fig. 8 Two paper models of the Bricard linkage

π (or greater than $-\pi$). For this model, the next Fig. 5 configuration can be (b) or (e), while (d) and (f) cannot be reached.

The locations of $A'BC$ and $A'B'C$ are determined by those of ABC' and $AB'C'$: ABC' and $A'B'C$ are on top at the same time, and so are $AB'C'$ and $A'BC$. Therefore, from the point $\sigma_1 = \sigma_2 = \pi$, each model must follow a unique and different branch of the c-space, as illustrated by Fig. 9, where the top and bottom half of the graph show the c-space parts attainable by the models in Figs. 8(b) and 8(a), respectively.

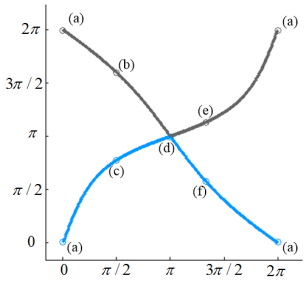

Fig. 9 Possible joint angles of the linkage paper models. Labeled points correspond to configurations shown in Fig. 5

Two reconfigurable mechanisms, Fig 10(a), each with three units, have been constructed by linking the two realizations of the Bricard linkage in Fig. 8(a) and 8(b). In the first mechanism, Fig. 10(a), only the model in Fig 8(a) is used. Both types of paper linkages are included in the second mechanism: two units as in Fig 8(a) at both ends, and one as in Fig 8(b) in the middle. Due to the physical constraints, each mechanisms can only trace a half-circle change of the joint angle σ_2 and move on a single c-space curve segment between two coplanar configurations. However, although the initial states of the two mechanisms are identical, all subsequent configurations for the same value of, say, σ_1 are distinct, and this includes the final collapsed states, Figure 10.

The case study illustrates well the possibility of realizing very different configuration space paths starting from the same state, and therefore shows potential use in the design of reconfigurable mechanisms. It also shows that physical-link interference can limit the choice of trajectories possible without reassembly. Therefore, during the mechanical design of the links and joints (not a subject of this paper) it must be carefully considered what panel shapes will allow the desired motions.

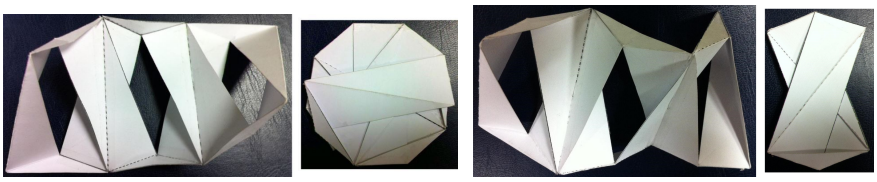

(a) (b)

Fig. 10 Possible movement of the two Bricard chain models

6 Conclusion

This paper presents the analysis of the configuration space and bifurcations of the type III Bricard linkage. Its bifurcation behavior is used to propose a novel family of reconfigurable mechanisms with such linkages as units. Through the kinematic analysis of the Bricard linkage, the dependence of two joint angles is derived, and the configuration space is described by the trajectory of a point of the linkage. Bifurcations on the configuration space are analyzed, and shown to provide the ability of the Bricard linkage to be used as a reconfigurable mechanism. By connecting pairs of unit linkages via scissor elements, a reconfigurable mechanism with a variable multi-furcating trajectory is built. The different motion sequences of a reconfigurable mechanism composed of three Bricard linkages have been illustrated by a model, validating the analysis.

Acknowledgements This research has been supported by the AUTORECON project funded under the Seventh Framework Program of the European Commission (Collaborative Project NMP-FOF-2011-285189), National Natural Science Funds (of China) for Distinguished Young Scholar under Grant 51125020, and the National Natural Science Foundation of China under Grant 51275015. The authors gratefully acknowledge the supporting agencies.

References

1. K. H. Hunt. *Kinematic geometry of mechanisms*. Clarendon Press Oxford, 1990.
2. P. T. Sarrus. Note sur la transformation des mouvements rectilignes alternatifs, en mouvements circulaires; et reciproquement. *Acad. Sci*, 36:1036–1038, 1853.
3. J. Phillips. *Freedom in machinery*, volume 2. Cambridge University Press, 2007.
4. R. Bricard. Mémoire sur la théorie de l'octaèdre articulé. *Journal de Mathématiques pures et appliquées*, 3:113–150, 1897.
5. J. E. Baker. An analysis of the Bricard linkages. *Mech Mach Theory*, 15(4):267–286, 1980.
6. Y. Z. Luo, Y. Yu, and J. J. Liu. A retractable structure based on Bricard linkages and rotating rings of tetrahedra. *Int. J Solids Struct*, 45(2):620–630, 2008.
7. Y. Chen and W. H. Chai. Bifurcation of a special line and plane symmetric Bricard linkage. *Mech Mach Theory*, 46(4):515–533, 2011.
8. M. Goldberg. Linkages polyhedral. *National Mathematics Magazine*, 16(7):323–332, 1942.
9. H. Lebesgue. Octaedres articulés de Bricard. *Enseign. Math. II*, 13:175–185, 1967.
10. A. V. Bushmelev and I. K. Sabitov. Configuration spaces of Bricard octahedra. *Journal of Mathematical Sciences*, 53(5):487–491, 1991.